Peer reviewed version

Link to publication record in Explore Bristol Research
PDF-document

University of Bristol - Explore Bristol Research
General rights

Extinction intensity during Ordovician and Cenozoic glaciations explained by cooling and paleogeography

Erin E. Saupe, Huijie Qiao, Yannick Donnadieu, Alexander Farnsworth, Alan T. Kennedy-Asser, Jean-Baptiste Ladant, Daniel J Lunt, Alexandre Pohl, Paul Valdes, Seth Finnegan

Table of Contents

S1. Methods

S1.1. Simulation overview. We used a cellular automaton algorithm that linked a gridded geographic domain with a one-dimensional temperature landscape[1-3] to test the effect of paleogeography, sea level drop, and temperature change on extinction magnitude during three climate transitions: Late Ordovician, Eocene–Oligocene and Plio–Pleistocene. The geographic component of the model consisted of a global 1°x1° grid of shallow marine continental shelf for each of the three time periods. We generated virtual species that occupied grid cells in these continental margins as a function of their assigned temperature tolerances and dispersal abilities. The one-dimensional climate landscape was perturbed, and the geographic response of the virtual species recorded (Fig. 2). The framework builds on the model introduced by Qiao et al.[1] and Saupe et al.[3], and is similar in concept to simulations explored by Rangel et al.[2] and Tomasovych et al.[4].

S1.2. Paleogeography. We isolated the effect of continental configuration on expected extinction magnitude for the three target periods using paleogeographic reconstructions from [5] for the Late Ordovician (450 Ma), from Scotese[6] for the late Eocene (~37 Ma), and from Robertson Plc. for the Pliocene[7] (mid-Pliocene Warm Period, ~3.1 Ma). The palaeogeographic reconstructions needed to match those used in the AOGCMs (see S.1.4) and therefore derive from different sources (e.g., Blakey *versus* Scotese). For each paleogeographic reconstruction, we used the shallow marine areas around terrestrial continental margins (Fig. 1; Fig. S2), excluding Antartica for the Eocene and Pliocene. We considered both narrow and broad marine shelves: the former was generated by extending all terrestrial continental margins by one cell (1°), whereas the latter was generated by extending terrestrial continental margins by three cells (Fig. 1; Fig. S2). The broad margin in particular may be broader than most marine shelfs, given resolution of the climate model data (1° is approx. 100 km at the equator).

    S.1.2.1. Simplistic hypothetical climate gradient. Only paleogeography differed across the time periods of interest in these simulations. For the analyses in which the magnitude of climate change was held constant across all intervals, we generated hypothetical 'warm climate' and 'cold climate' temperature gradients by averaging interval-specific ocean-atmosphere general circulation models (AOGCMs). The 'warm' gradient was generated by calculating the average temperature by absolute latitude from AOGCMs for the Late Ordovician FOAM v.1.5, Eocene FOAM v.1.5, and Pliocene HadCM3BL (Robertsons). Average values per degree absolute latitude were used to generate a symmetrical gradient (Fig. S3). The 'cold' gradient was generated in the same fashion by calculating the average temperature by absolute latitude from icehouse AOGCMs for the Late Ordovician FOAM v.1.5, Oligocene FOAM v.1.5, and Pleistocene HadCM3BL (Robertsons). These average gradients capture the general aspects of the distribution of sea surface temperatures that are common to all warm or cold climate states.

    S1.2.2. Virtual species. Virtual species were generated at every possible shallow marine cell bordering land in each paleogeographic reconstruction, for a total of 2233, 2258, and 2892 virtual species for the Ordovician, Eocene, and Pliocene, respectively. Consequently, the number of species by latitude was dictated by paleogeography, such that no diversity gradient was enforced. Each simulation focused only on one virtual species. Thus, multiple species (i.e., those with different niches/dispersal abilities) could not occupy the same cell within a given simulation. A virtual species began the simulation at one of the 'seed' cells defined above: the temperature value of the seed cell defined the optimal environmental conditions for that species (i.e., the center of the species' niche). From this

value, symmetrical deviations were applied[1,2] based on a narrow and broad niche breadth, corresponding to temperature tolerances of 8° and 12°, respectively. These niche breadths, although roughly representative of thermal tolerances of marine ectotherms, may be broader than many living tropical marine species[4,8,9].

Each species was assigned a dispersal function, reflecting its ability to search for habitable cells from its point of origin. We considered two dispersal abilities: poor and good. Poor dispersers could search only one cell in a given simulation time step from every cell currently occupied. Each cell occupied by a species searched for suitable habitat in all directions. Since poor dispersers could search only one cell in a given time step, they were limited to searching the four cardinal directions only. Species could search any cell, regardless of whether that cell was suitable to the species (i.e., within their thermal tolerance). However, at the end of a time step, species could occupy only suitable cells, and therefore poor dispersers were prohibited from jumping over unsuitable regions, regardless of the number of dispersal attempts.

Good dispersers were represented by an exponential decay curve, defining the probability that a species would disperse a certain number of cells (Table S1). Each cell occupied by a good disperser was assigned a different probability of searching a set number of cells (i.e., a search radius). This search radius was selected randomly from the probabilistic exponential decay function and capped at eight for any given cell within a single simulation time step (see Table S1). From a given cell, a species could then search for suitable cells in all directions up to the specified radius. Good disperses could therefore jump over unsuitable patches to encounter more spatially remote, but suitable, cells elsewhere. As with poor dispersers, a good disperser could search unsuitable cells, but they could only occupy suitable cells at the end of a time step. The probability that a species searched up to eight cells was low; instead, it was more likely a species searched only one or two cells, for example.

Poor and good dispersers searched for suitable cells simultaneously from all cells currently occupied. Dispersal values were based loosely on known dispersal abilities in marine bivalves[10,11]. Dispersal in this formulation is stochastic and represents a process of exploration, with possible colonization and range expansion, and thus differs from other definitions of dispersal at local scales, such as movements of individuals.

S.1.2.3. Climate cooling. For each simulation, warm 'greenhouse' conditions were initially held constant so that the incipient species could expand its geographic range. Species searched for suitable habitat based on their assigned dispersal ability for a total of 40 time steps. This 'burn in' period was sufficient for species to become equilibrated with the warm climate and for simulations to stabilize, after which icehouse conditions were immediately enforced (i.e., the change to cold conditions occurred in a single time step). Throughout the burn in period, species occupied any *suitable* cell encountered in the dispersal process. The dispersal process was intended to imitate the natural range dynamics of species, which often begin small and expand subsequently[12,13].

The transition from a warm to cold climate modified the distributions of suitable cells uniquely for each virtual species, dependent on niche dimensions. Species tracked suitable cells as a function of their dispersal ability. We allowed 40 time steps for species to track and occupy suitable habitat once the climate had cooled. A virtual species went extinct if it was unable to occupy any suitable cells after this period. We follow Qiao et al.[1] in applying no specific demographic model or inferred minimum population survivorship threshold. A strict extinction criterion was used because it invoked the fewest assumptions, and because we were cognizant of the relatively coarse spatial resolution of the simulation.

Each virtual species in each continental configuration (Late Ordovician, Eocene and Pliocene) was tested under all combinations of niche (narrow and broad), dispersal ability

(poor and good), and marine shelf area (broad and narrow), for a total of 52,824 individual simulations. We quantified the number of species that went extinct for each continental configuration for each simulation combination.

S.1.3.4. Statistical tests. Generalized linear models (GLM) assuming a binomial distribution of errors and a logit link function were used to test for statistical differences in proportional extinction generated by the paleogeography. Models for each unique simulation combination were assessed for over-dispersion and residuals checked for heteroscedasticity and bias. Planned post-hoc comparisons were implemented to assess statistical differences between factor levels (i.e., continental configuration of the three time periods) using the 'glht' function in the 'multcomp' package for R[14]. All *p*-values were adjusted for multiple comparisons based on the single-step method (Table S5).

We tested for the effect of coastline orientation and 'island' occupation on extinction probability. Proportional extinction was quantified on east-west coastlines and on 'islands' and compared to proportional extinction on north-south coastlines (Fig. 4). Our expectation was that proportional extinction would be higher on 'islands' and east-west-oriented coastlines, because species inhabiting these regions would not be able to track suitable habitat as effectively when climate (specifically temperature) changed. 'Islands' were defined as small isolated shallow marine shelf areas with contiguous cells, identified using the 'dbscan' package[15] in the R programming language v.3.3.1. We examined only the effect of small 'islands', since the entirety of a small 'island' is more likely to become unsuitable for a given species with climate change and to prohibit habitat tracking. We therefore selected only those 'islands' containing fewer than 105 cells (see Fig. S18). Coastline direction was defined using a script that identified the neighbors of a given cell. If a cell had neighbors to the east and west, the cell was assigned as an east-west coastline. If a cell had neighbors to the north and south, it was assigned as a north-south coastline. If a given cell had both north-south and east-west neighbors, it was assigned as a 'corner' cell and excluded from analysis (Fig. S18). We examined patterns only using the narrow marine shelf definition, since the internal cells in the broad marine shelf would be difficult to assign to a particular coastline orientation (i.e., these cells would be included in both north-south and east-west coastlines). We considered patterns when excluding and including the 'tropical extinction zone'; this zone occured because of the static niches employed in our simulation framework. Species within this zone were 'destined for extinction' when climate cooled, since no suitable habitat remained available to them. Results were similar regardless of whether we included or excluded this extinction zone, and therefore we focus only on the former. Finally, we awknowledge that all minor variations in coastline direction are not necessarily real, given paleogeographic uncertainties. However, the method used to identify coastline orientation is likely effective for the specific paleogeographies used in our simulations.

S.1.3. Sea level. Using the simulation framework defined above, we evaluated the degree to which glacioeustatically-driven changes in sea level during each of the three climatic transitions (Late Ordovician, Eocene–Oligocene, and Plio–Pleistocene) could have produced differential extinction magnitudes. As in previous simulations, gridded regions were defined by extending terrestrial continental margins by one or three cells to represent narrow and broad shelf habitats, respectively. However, in the new simulations, we shifted these gridded regions from their position in a greenhouse world to their position in an icehouse world, reflecting estimated changes in sea level from glacial growth. Shelf habitats, however, remained a width of either one or three cells.

The paleogeographies from the first simulation were used to characterize greenhouse conditions for the Late Ordovician, Eocene, and Pliocene. Shallow marine areas during

icehouse conditions were then isolated by dropping sea level for the Ordovician and Eocene (methods detailed below) and using the Pleistocene paleogeographic reconstruction from Robertson Plc.[7]. Therefore, in these simulations, the climate transitioned from warm to cold, *and* the position of the marine shelf itself changed.

Mean eustatic sea level fall for the Late Ordovician is approximated at 200 m[16-18], whereas mean eustatic sea level fall provoked by the Eocene-Oligocene glaciation has been estimated at ~70-80 m from paleoceanographic records[19-21], stratigraphic records[22], and model simulations[23-25]. Consequently, we estimated sea level drop by subtracting 200 m from every grid cell in the Late Ordovician paleogeography of [5], and by subtracting 75 m from every grid cell in the late Eocene paleogeography of Scotese[6]. Doing so led to a change in the global land–sea mask, since oceanic grid points become continental if their bathymetry is lower than mean sea level fall. Adding a uniform eustatic sea level fall remains, of course, an approximation of true variations of sea level generated by the emplacement of ice sheets at the poles. This approximation occurs because glacial isostatic adjustment is inherently non-uniform at the global scale[25-27], although the far-field sea level fall is relatively close to the eustatic mean.

Aside from shifting the position of shallow marine habitat (i.e., sea level change), simulations differed from the previous round only in the mechanism used to account for the changed position of the marine shelf: a virtual species could disperse to the shelf post-sea-level-drop as a function of distance from the shelf pre-sea-level-drop, combined with species' dispersal ability (Table S1). That is, in some regions sea level change caused a large offset in the shallow marine shelf, whereas in other regions the position of the shelf remained similar. To keep the simulation framework simple, we invoked 'jump' dispersal to new coastlines, rather than attempt to estimate rates of sea level drop. We examined patterns when species were allowed one chance (Fig. S7) to jump to the new marine shelf position based on their assigned dispersal ability, and when they were allowed five chances (Fig. S8); species went extinct if they failed these attempts. When species were allowed one attempt, poor dispersers could reach the new shelf only if its new position was contiguous with the old, since poor dispersers could search only one cell in a time step. If species reached the new shelf area, they searched for suitable habitat for 40 time steps, similar to the previous round of simulations.

Each virtual species in each climatic transition (Late Ordovician, Eocene–Oligocene and Pliocene–Pleistocene) was tested under all combinations of niche (narrow and broad), dispersal ability (poor and good), and marine shelf area (narrow and broad), for a total of 52,824 simulations. We tallied number of simulated species that went extinct for each unique simulation combination. The statistical framework described above was employed to test for differences in proportional extinction among the three climatic transitions, which would have resulted from the combined effect of paleogeography and changes in sea level (Table S5).

S.1.4. Temperature. We relied on mean annual sea surface temperature estimates from AOGCMs to test the effect of estimated cooling on extinction magnitude for three greenhouse-icehouse transitions (Late Ordovician, Eocene–Oligocene and Pliocene–Pleistocene). Thus, this simulation round relied on modeled changes in temperature across each greenhouse- icehouse transition instead of the artificial temperature gradients used in the previous simulations, whilst also accounting for differences in paleogeography, greenhouse gasses, and sea level. All other details of the simulation framework remained the same. We took a deliberately simplistic approach that did not account for differences in rates of change, which are difficult to constrain in the deep-time record, but instead used "before" and "after" estimates of global mean sea surface temperature.

To validate our choice of models, we compared modelled tropical surface temperature changes to changes inferred from proxy datasets spanning each greenhouse-icehouse transition. We limited the model-proxy comparison to tropical surface temperatures because, for the Late Ordovician, direct proxy constraints are only available for the shallow tropical Anticosti Basin[16,28]. Although modelled changes slightly exceed changes inferred from proxy data, the ~ -7° C drop in temperature inferred from clumped isotope analysis of latest Ordovician fossils in the Anticosti Basin substantially exceeds the estimated -3° C change in mean tropical surface temperature across the Eocene-Oligocene transition [29] and the similar average change observed across the Pliocene-Pleistocene transition[30] (Fig. S14).

We compared proportional extinction for each climate transition within the *same* AOGCM model, except when this was not possible—e.g., the Ordovician, for which we only had access to the FOAM model. The temperature change for the Late Ordovician was represented by one AOGCM combination; for the Eocene–Oligocene by three AOGCM combinations; and for the Pliocene–Pleistocene by two AOGCM combinations (described in detail in S3).

Virtual species were generated at every possible shallow marine cell bordering land for each AOGCM (see Table S2 for virtual species numbers). Each virtual species in each greenhouse-icehouse model combination was tested under all variations of niche (narrow and broad), dispersal ability (poor and good), and marine shelf area (narrow and broad). We counted the number of virtual species that went extinct for each unique simulation combination. Proportional extinction resulting from the simulation framework was compared statistically amongst the three climate transitions by considering four AOGCM model pairings (see Table S5) and the same framework described above. Details of AOGCMs are provided in Table S3.

S.1.5. Defining the shallow marine shelf. To test for the effect of continental flooding and extent of shallow marine shelf area on extinction magnitude across the three climate transitions, simulations were run using a definition of shallow marine as cells within 0 to 200 m water depth (see Fig. S4). We chose 200 m as the depth threshold because it represents the bottom of the photic zone, even in very oligotrophic conditions. Cells were isolated from palaeogeographies using the associated bathymetric data. Virtual species were generated at each of these cells (see Table S4 for numbers). Species could search for suitable habitat within the extent of this shallow marine area based on their dispersal ability. The same simulation framework described above was then used to test for the effect of (i) paleogeography alone, (ii) paleogeography and sea level drop, and (iii) paleogeography, sea level drop, and temperature change on extinction magnitude across the greenhouse to icehouse transitions. When testing paleogeography alone, the position and extent of shallow marine area stayed the same from greenhouse to icehouse conditions, and only temperature dropped via the artificial climate gradients. In remaining simulations, however, the position *and* extent of the marine shelf changed to simulate changes in continental flooding (see Fig. S4). Results from these simulations were congruent with previous rounds that defined shallow marine regions as cells bordering land (Fig. 1; Fig. S2), and thus we focus our discussion and analyses on the latter.

Table S1—Values used to calculate dispersal distances in the simulations

# of cells	1	2	4	6	8
Poor dispersers	1	0	0	0	0
Good dispersers	0.3766	0.3476	0.2524	0.0229	0.0004

Table S1. Values used to calculate the number of cells searched in a time step. Poor dispersers always searched one cell in a given time step from all cells currently occupied. Good dispersers, however, searched a variable number of cells: for each time step and occupied cell, a number was drawn randomly from 0 to 1, representing the probability that the species would disperse a given number of cells. Thus, if a value of > 0.9996 was drawn for a given time step and cell (probability of < 0.0229), the species from that cell would be allowed to search 6 cells.

Table S2—Number of virtual species used for each AOGCM combination

Climate transition	Climate model codes	Climate model details	# of virtual species (seeds)
Late Ordovician	[1-2]	FOAM v.1.5	2233
Eocene – Oligocene	[3-6]	Getech HadCM3(L)	3490
	[4-7]	Roberston HadCM3(L)	3456
	[5-8]	FOAM v.1.5	2258
Pliocene – Pleistocene	[9-11]	Getech HadCM3(L)	2310
	[10-12]	Roberston HadCM3(L)	2892

Table S2. The number of virtual species used for each AOGCM combination. Virtual species were generated (i.e., simulations initiated) at every possible shallow marine cell bordering land in each paleogeographic reconstruction. The AOGCMs used to represent each climate transition for the Late Ordovician, Eocene–Oligocene, and Pliocene–Pleistocene are represented in square brackets, with model details provided in Table S3.

S3: Ocean-atmosphere general circulation model (AOGCM) details

Table S3. Details of global climate models (AOGCMs) used in the simulations. The following models were paired to represent the transition from greenhouse to icehouse conditions for each time period: [1] to [2] for the Late Ordovician; [3] to [6], [4] to [7], and [5] to [8] for the Eocene–Oligocene; and [9] to [11] and [10] to [12] and for the Pliocene–Pleistocene.

	Climate model code	Time period	Climate state	Climate model (AOGCM) details	Solar constant (W/m²)	Atmospheric CO_2	Length of run	Reference
Late Ordovician	1	pre-Hirnantian	Greenhouse	Asynchronous coupling btwn FOAM v.1.5, LMDZ & GRISLI	1319	2240 ppm	At equil.	[18]
	2	Hirnantian	Icehouse	Asynchronous coupling btwn FOAM v.1.5, LMDZ & GRISLI	1319	840 ppm	At equil.	[18]
Eocene – Oligocene	3	Ypresian (Getech)	Greenhouse	HadCMBL	1358.91	1120 ppm	1422	[31]
	4	Ypresian Roberstons	Greenhouse	HadCM3BL	1358.91	560 ppm	At equil.	[7]
	5	Eocene/Oligocene Transition	Greenhouse	Asynchronous coupling btwn FOAM v.1.5, LMDZ & GRISLI	1361	1120 ppm	2000	[23]
	6	Oligocene – Rupelian (Getech)	Icehouse	HadCM3BL	1361.35	560 ppm	1422	[31]
	7	Oligocene – Chattian (Roberstons)	Icehouse	HadCM3BL	1361.35	280 ppm	At equil.	[7]
	8	Eocene/Oligocene Transition	Icehouse	Asynchronous coupling btwn FOAM v.1.5, LMDZ & GRISLI	1361	560 ppm	2000	[23]
Pliocene – Pleistocene	9	Piacenzian (Getech)	Greenhouse	HadCM3BL	1364.73	400 ppm	1422	[31]
	10	Pliocene - Non-specific (~3 Ma; Roberstons)	Greenhouse	HadCM3BL	1365.00	401 ppm	At equil.	[7]
	11	Pleistocene (LGM; Getech)	Icehouse	HadCM3BL	1364.89	180 ppm	1422	[31]
	12	Pleistocene (LGM; Robertsons)	Icehouse	HadCM3BL	1365.00	185 ppm	At equil.	[7]

A description of the AOGCMs used in this study is provided in section S3.1 and indicated by a number in square brackets, which can be referenced back to Table S3. We employed two different AOGCMs of differing complexities in order to evaluate uncertainty in predicted extinction magnitude resulting from model choice. We also tested the relative impact of different paleogeographic reconstructions (Getech Group Plc. [3] and [6], and Robertsons Plc. [4] and [7]) within the same model (HadCM3BL) (Table S3).

Experiment-specific boundary conditions for AOGCMs were paired to represent the greenhouse-icehouse transitions for each of three time periods (Late Ordovician, Eocene–Oligocene, and Pliocene–Pleistocene). The greenhouse-icehouse transition for the Late Ordovician was represented by one AOGCM combination ([1 to 2]), the transition for the Eocene–Oligocene by three AOGCM combinations ([3 to 6], [4 to 7], and [5 to 8]), and the transition for the Pliocene–Pleistocene by two AOGCM combinations ([9 to 11] and [10 to 12]), see Table S3.

S3.1 Models: (i) HadCM3BL

    We employed HadCM3BL[32], an AOGCM, which is a version of the UK Met Office Model, HadCM3. The atmosphere and ocean component of HadCM3BL runs at a resolution of 3.75° x 2.5° longitude by latitude with 19 hybrid vertical levels in the atmosphere and 20 depth levels in the ocean. A dynamic vegetation model, TRIFFID (Top-down Representation of Interactive Foliage and Flora Including Dynamics; [33]), was utilized alongside the MOSES 2.1a land surface scheme[34]. TRIFFID predicts the distribution of vegetation using a plant functional type (PFT) approach for 5 different PFTs: broadleaf trees, needleleaf tree, C3 grass, C4 grass and shrubs. Grid-boxes are fractional and can contain a mixed coverage. HadCM3BL has been used for a wide range of paleoclimate studies of the Paleogene[31,35,36] and is computationally 'fast', which is required to run long integrations when simulating past climate states. This allows simulations to reach near-equilibrium in at least the surface and mid-ocean[31], while still being a full-complexity model. For more detailed information, see Valdes et al.[32]. HadCM3BL has been used extensively in the Coupled Model Intercomparison Project (CMIP) 3 and 5, performing comparably to many higher-fidelity CMIP5 models when compared to observations[32].

    S3.1.1 Boundary conditions

    Mid-point, stage-specific boundary conditions were utilized. Paleogeographic reconstructions were provided by both Getech Group Plc.[31] and Robertsons Plc.[7,37] for the Ypresian (Eocene), Rupelian and Chattian (Oligocene), Piacenzian (Pliocene), and Pleistocene. Stage mid-point-specific solar constants (after the model of stellar evolution[38]), CO_2, and prescribed ice sheet reconstructions for each simulation are shown in Table S3. Simulations using a Getech paleogeography assigned CO_2 concentration in line with most recent estimates[39-42]. Simulations for each paleogeography were run for 1,422 model years using a consistent four-stage initialization and spin-up approach with geologic stage-specific boundary conditions[31]. Simulations using the Roberston paleogeography have a longer spin-up than the Getech simulations, typically having been run until there is negligible energy imbalance at the top of the atmosphere (<0.1 W m^{-2}) and until little to no trend in the volume integrated ocean temperatures (<0.1 °C drift over 1,000 years). Lastly, we kept a modern-day orbital configuration for all simulations to remove the impact of orbital variability, making stage-to-stage comparisons possible.

    S3.1.2 Initial conditions

     The Getech HadCM3BL simulations used a generic initialization procedure, whereby the ocean was set as stationary, zonal mean temperature structure of the ocean was determined by the cosine function of latitude (see Lunt et al.[31] for details), and a constant salinity of 35 psu was employed. The atmosphere was initialized from a previously-equilibrated, pre-industrial state. Land surface initial conditions were also set to a globally homogenous state. Ozone concentrations were diagnosed based on the simulation specific tropospheric height as a 3-D varying field. The Robertsons simulations are continuations of other, older paleoclimate model runs. The older runs were originally initialized with a pre-industrial ocean, with variables extrapolated to fill gaps each time the paleogeography was changed.

S3.2 Models: (i) FOAM v.1.5

    We used an asynchronous coupling method between a mixed-resolution AOGCM (FOAM version 1.5[43]), an up-to-date AGCM (LMDZ[44]), and a high-resolution ice-sheet model (GRISLI[45]) to simulate Eocene and Ordovician land-ice configurations in equilibrium with global climate. Comprehensive descriptions of the experimental setups are provided by

Ladant et al.[23] and Pohl et al.[18]. Fields of sea-surface temperatures used in the present study were simulated using the FOAM AOGCM, which has been used extensively for paleoclimate studie[23,46,47]. The atmospheric component of the FOAM model is a parallelized version of the National Center for Atmospheric Research's (NCAR) Community Climate Model 2 (CCM2), with the upgraded radiative and hydrologic physics from CCM3 version 3.2[48]. It runs at a R15 spectral resolution (4.5° × 7.5°) with 18 vertical levels. The oceanic module is the Ocean Model v.3 (OM3), a 24-level z-coordinate ocean GCM running at a resolution of 1.4° × 2.8°. A sea-ice module is also included, which uses the thermodynamic component of the CSM1.4 sea ice model, the latter being based on the Semtner 3-layer thermodynamic snow/ice model[49]. The FOAM model is well designed for paleoclimate studies: it has no flux correction and its quick turnaround time allows for long, millennium-scale integrations.

S3.2.1 Boundary conditions

Ordovician. We used the Late Ordovician continental reconstruction from Blakey[5]. Ordovician vegetation was restricted to nonvascular plants[50,51], the coverage of which is difficult to estimate and currently debated[52,53]. Therefore, we followed previous studies regarding Ordovician climate[54-56] in imposing a bare soil (rocky desert) on landmasses. The solar luminosity was set to its Ordovician level (i.e., –3.5% compared to its present-day value; Gough et al., 1981). Simulations were run at several atmospheric CO_2 levels (2800 ppm, 2240 ppm and 840 ppm CO_2) for two opposite orbital configurations: 'Hot Summer Orbit' (HSO) and 'Cold Summer Orbit' (CSO)[18].

Eocene. We used the a late Eocene to early Oligocene paleogeography from [6], with refinements in the Tethys[57] and Central American seaways, as in Lefebvre et al.[58]. The Antarctic continent for the Eocene was updated using the recent maximum paleotopographic estimate from Wilson et al.[59], and the paleobathymetry follows Bice et al.[60]. Four simulations from Ladant et al.[23] were used in this study. Two with 1120 ppmv CO_2, no ice sheet over Antarctica, and either a Cold Summer Orbit (CSO) or a Warm (or Hot) Summer Orbit (HSO), to represent pre-EOT conditions, and two with 560 ppmv CO_2, a full Antarctic ice sheet, and either CSO or HSO configurations to represent post-EOT conditions.

S3.2.2 Initial conditions

Ordovician simulations were initialized with present-day potential temperature and salinity fields. Eocene-Oligocene simulations were initialized with modern salinity fields and present-day+9°C or present-day+11°C fields for 560 ppmv and 1120 ppmv simulations, respectively. Both Ordovician and Eocene-Oligocene simulations were then run for several thousand model years until thermal quasi-equilibrium of the ocean (global mean temperature drift < 0.1°C/century).

S3.3. AOGCM parameter choices made for ecological modelling

S3.3.1 Late Ordovician FOAM v.1.5

We considered simulations run at several atmospheric CO_2 levels (10x, 8x, and 3x PAL). Based on the results of the model-proxy comparison conducted by Pohl et al.[18], the former two thresholds (10x and 8x PAL) were selected to reflect climatic conditions prevailing during pre-Hirnantian times (~450 Ma), whereas the latter (3x PAL) was selected to represent the latest Ordovician Hirnantian glacial peak (~445 Ma). Results were similar for the transition from 10x to 3x PAL and from 8x to 3x PAL, and thus we focus here only on the latter; this approach is conservative, as it reduces the chance of a type I error (i.e., explaining the high rate of extinction during the Ordovician as a function of temperature change when it

perhaps was not a causal factor), since invoking less temperature change (8x to 3x PAL *versus* 10x to 3x PAL) will result in fewer extinctions in which to compare to the other greenhouse to icehouse transitions. We used an average of the two orbital scenarios (CSO and HSO), but results do not differ if scenarios are considered individually. The native resolution of the data was downscaled to 1°x1° using bilinear interpolation.

S3.3.1 Eocene & Oligocene FOAM v.1.5

We used an average of the HSO and CSO scenarios, but results did not differ if scenarios were considered individually. The native resolution of the data was downscaled to 1°x1° using bilinear interpolation.

S3.3.2 Eocene (Ypresian) HadCM3BL

We chose the Ypresian to represent greenhouse climate conditions, since this stage represents the first and warmest of the Eocene[61], and we sought more extreme differences in paleogeography to compare to Pliocene paleogeography. We tested two different AOGCM simulations, with CO_2 forcing at 1120 ppm and 560 ppm, in our ecological modelling. Results were broadly consistent using both CO_2 thresholds, and thus we present only those for 1120 ppm; this approach is conservative, since it results in a greater temperature drop from the Eocene to Oligocene, and thus higher rates of extinction in which to compare to the extremely high rates observed during the Late Ordovician, reducing the chance of a type I error (i.e., explaining the high rate of extinction during the Ordovician as a function of temperature change when it was perhaps not a causal factor). The native resolution of the data was downscaled to 1°x1° using bilinear interpolation.

S3.3.3 Oligocene (Rupelian/Chattian) HadCM3BL

We tested three different AOGCM simulations, with CO_2 forcing at 840, 560, and 280 ppm, in our ecological modelling. Results were broadly consistent using all three CO_2 thresholds, and thus we present only those for 560 ppm (Rupelian) and 280 ppm (Chattian); this approach is conservative, since it results in a greater temperature drop from the Eocene to Oligocene, and therefore higher rates of extinction in which to compare to the extremely high rates observed during the Late Ordovician, thus reducing the chance of a type I error (i.e., explaining the high rate of extinction during the Ordovician as a function of temperature change when it was perhaps not a causal factor). The native resolution of the data was downscaled to 1°x1° using bilinear interpolation.

Table S4—Number of virtual species used for each AOGCM combination, using a shelf definition of 0–200 m water depth

Climate transition	Climate model codes	Climate model details	# of virtual species (seeds)
Late Ordovician	[1-2]	FOAM v.1.5	7056
Eocene – Oligocene	[3-6]	Getech HadCM3(L)	4710
	[4-7]	Roberston HadCM3(L)	4223
	[5-8]	FOAM v.1.5	3711
Pliocene – Pleistocene	[9-11]	Getech HadCM3(L)	2502
	[10-12]	Roberston HadCM3(L)	2579

Table S4. The number of virtual species used for each AOGCM combination when considering shallow marine shelf area as cells within 0 to 200 m water depth. Virtual species were generated at each of these cells (Fig. S4). The AOGCMs used to represent climate transitions for the Late Ordovician, Eocene–Oligocene, and Pliocene–Pleistocene are represented in square brackets, with model details provided in Table S3.

Table S5—Post-hoc comparison results

		Good dispersal				Poor dispersal			
		Broad NB		Narrow NB		Broad NB		Narrow NB	
		Ord/E	Ord/P	Ord/E	Ord/P	Ord/E	Ord/P	Ord/E	Ord/P
Continental configuration only (artificial temperature gradient)									
Narrow shelf	Artificial temperature drop	1.68	2.05	10.59	5.62	**-1.40**	**-1.67**	**2.81**	5.92
Broad shelf	Artificial temperature drop	1.66	1.99	11.86	7.20	**0.17**	-2.89	**4.24**	2.33
Continental configuration & change in continental flooding (artificial temperature gradient)									
Narrow shelf	Artificial temperature drop	**0.47**	1.48	10.82	6.14	22.53	23.85	14.95	16.91
Broad shelf	Artificial temperature drop	1.08	1.37	12.09	6.30	7.77	4.46	8.86	5.39
Global climate model scenarios									
Narrow shelf	Ord [1-2]; E-O [3-6]; Plio-Pleis [9-11]	21.88	25.14	35.28	38.13	22.22	34.56	33.15	47.08
	Ord [1-2]; E-O [4-7]; Plio-Pleis [10-12]	21.44	25.04	26.78	28.47	17.26	31.90	21.58	27.55
	Ord [1-2]; E-O [5-8]; Plio-Pleis [10-12]	25.66	25.04	39.95	28.47	35.60	31.90	49.05	27.55
	Ord [1-2]; E-O [5-8]; Plio-Pleis [9-11]	25.66	25.14	39.95	38.13	35.60	34.56	49.05	47.08
Broad shelf	Ord [1-2]; E-O [3-6]; Plio-Pleis [9-11]	16.52	15.96	36.38	35.48	21.59	27.17	35.44	41.08
	Ord [1-2]; E-O [4-7]; Plio-Pleis [10-12]	15.10	15.97	33.54	30.02	21.35	25.17	26.27	24.91
	Ord [1-2]; E-O [5-8]; Plio-Pleis [10-12]	16.52	15.97	37.21	30.02	28.21	25.17	43.54	24.91
	Ord [1-2]; E-O [5-8]; Plio-Pleis [9-11]	16.52	15.96	37.21	35.48	28.21	27.17	43.08	41.08

Table S5. Results from post-hoc comparisons that assess statistical differences in proportional extinction (expressed as percentages for ease of reading) between each of the greenhouse-icehouse transitions resulting from: (i) continental configuration alone, (ii) continental configuration and change in sea level; and (iii) interval-specific and paleogeographically-explicit sea surface temperature change estimates from AOGCMs. Reported values represent differences in proportional extinction between the Late Ordovician and the Eocene–Oligocene transitions (Ord/E), and between the Late Ordovician and Plio-Pleistocene transitions (Ord/P); bold values indicate insignificant tests with $p > 0.05$. Numbers in square brackets on the left refer to AOGCMs used to represent each greenhouse-icehouse transition (see Table S3). E-O = Eocene–Oligocene transition; Ord = Late Ordovician transition; Plio-Pleis = Pliocene–Pleistocene transition).

Figure S1— The influence of paleogeography on extinction in two hypothetical worlds
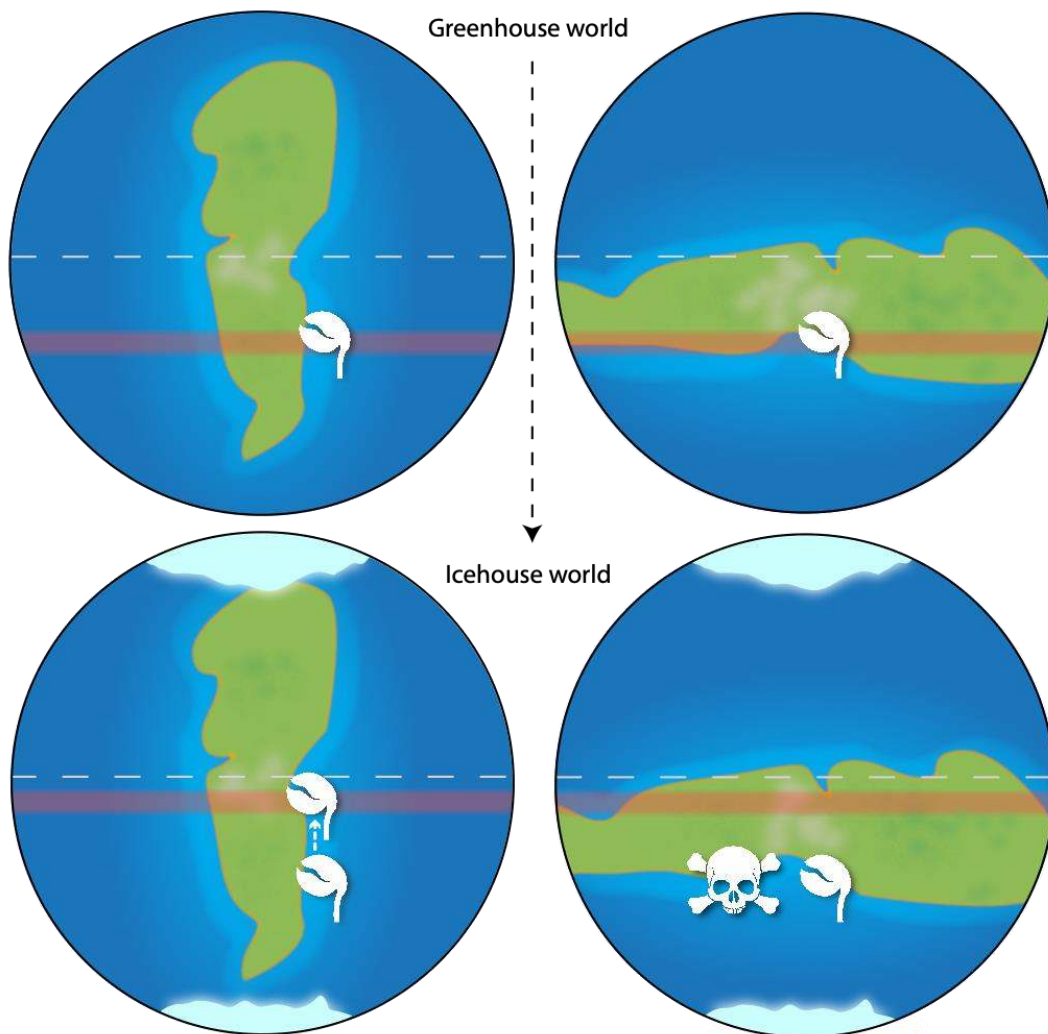

Figure S1. The influence of paleogeography on extinction in two hypothetical worlds with either a single continent that spans from the north to the south pole (left column) or a single circum-equatorial continent that blocks dispersal from either the north or south (right column). The species' thermal tolerance is represented by the light pink band, and its distributional range by the brachiopod symbol. As climate transitions from warm (top row) to cold (bottom row), the species' thermal niche shifts equatorward. The shallow-marine-restricted species along the north-south oriented continent would be able to track its thermal niche. However, the shallow-marine-restricted species along the east-west oriented continent would have no such option and would be driven to extinction. We hypothesize that the geographic arrangement of continental crust may be important in regulating extinction risk, since it has the potential to facilitate or inhibit habitat tracking during periods of climate change.

Figure S2—Per-cell proportional extinction for each greenhouse-icehouse transition
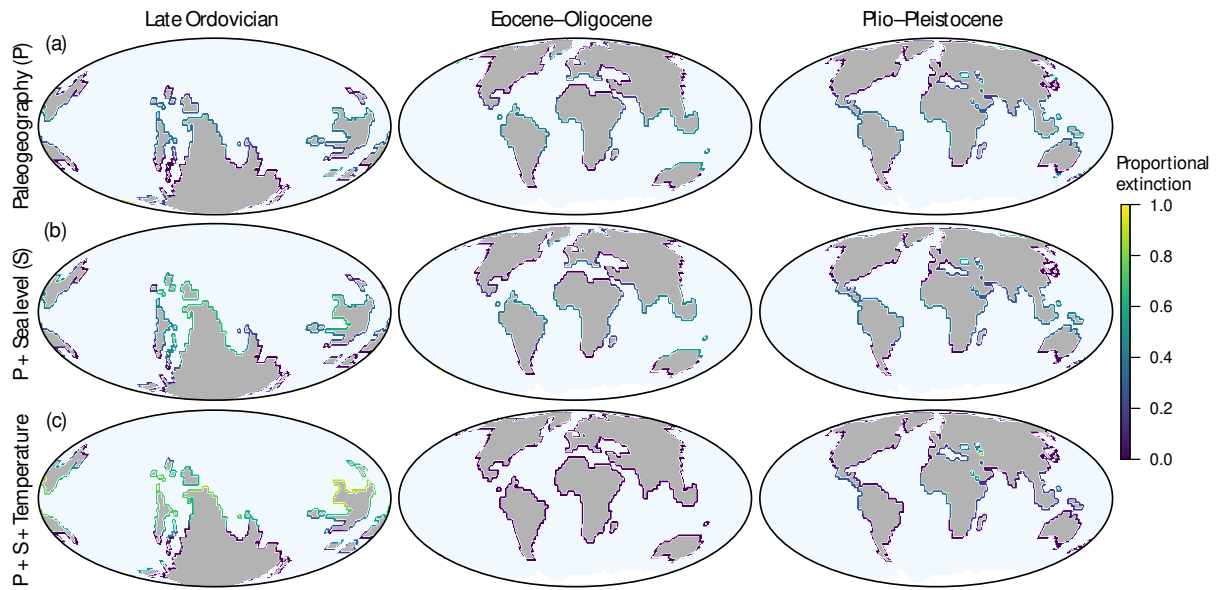

Figure S2. Per-cell proportional extinction for each greenhouse-icehouse transition, for simulations isolating the effect of paleogeography (a), paleogeography and sea level change (b), and the aforementioned factors including temperature change, aside for the FOAM climate models (c). Results show the average extinction across all dispersal and niche scenarios under the narrow continental shelf. Temperature change was represented by the FOAM climate model for the Late Ordovician and Eocene–Oligocene, and by the Robertson HadCM3BL climate model for the Plio–Pleistocene (see Table S3 for details). Proportional extinction was higher on islands and in equatorial regions, and lower along long north-south coastlines.

Figure S3—Artificial temperature gradients used in the simulations

(a) Artificial climate gradient representing 'warm condtions'
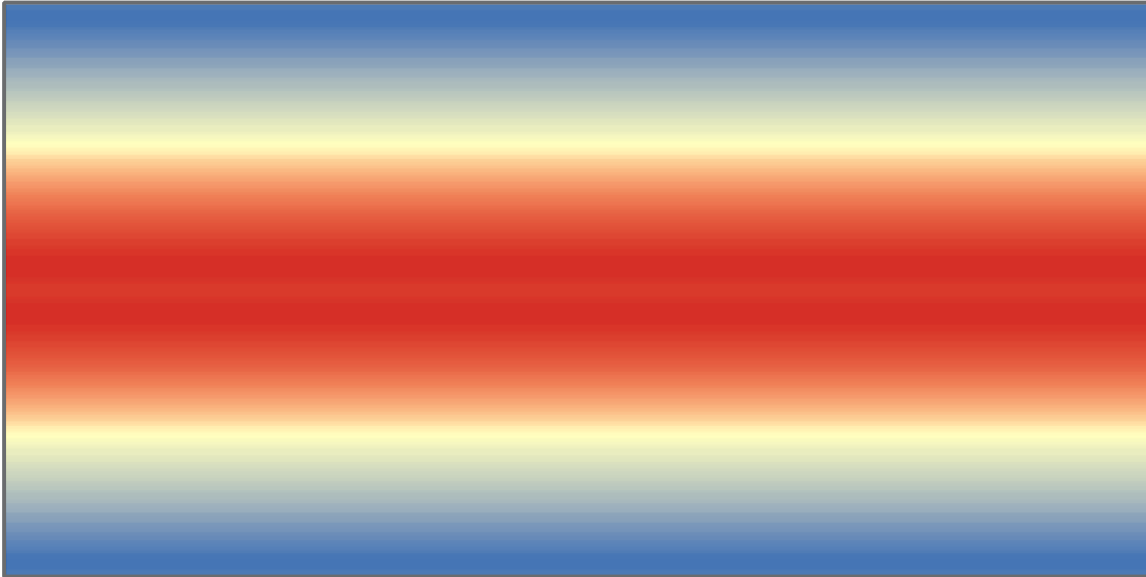
(b) Artificial climate gradient representing 'cool condtions'
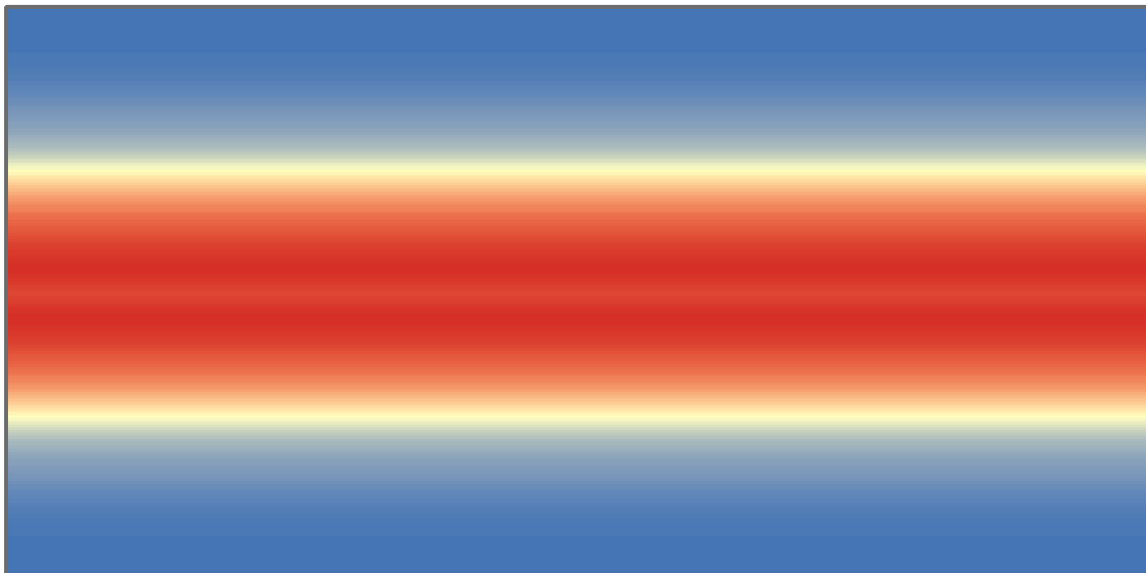
Figure S3. Artificial temperature gradients generated by averaging interval-specific ocean-atmosphere general circulation models (AOGCMs). Methodological details are provided in S.1.2.1. The 'warm' climate layer (a) was characterised by temperatures of 31.10°C at the equator (dark red) and 0.19°C at the poles (blue), whereas the cold layer (b) was characterised by temperatures of 25.65°C at the equator (dark red) and -1.67°C at the poles (blue). The shallow marine margins around continents during the Late Ordovician, Eocene–Oligocene, and Pliocene–Pleistocene were used as templates to extract the regions in which the simulations were run (see Fig. 1 and Fig, S2).

Figure S4—Extent of simulated area, 0 to 200 m water depth definition
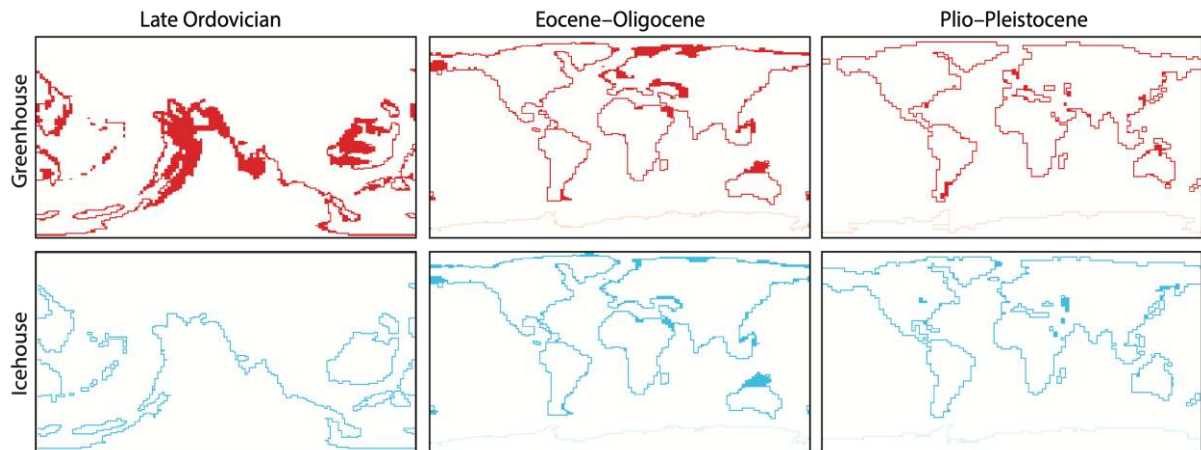
Figure S4. The regions in which simulations were run obtained by selecting cells within 0 to 200 m water depth. Species could search for suitable habitat within this shallow marine area based on their dispersal ability. Simulations that considered paleogeography alone used the extents from greenhouse conditions (top row) only. The extent and position of the marine shelf changed in simulations testing for the role of paleogeography and sea level drop, and in simulations that incorporated interval-specific and paleogeographically-explicit surface temperature change estimates from AOGCMs (bottom row, icehouse conditions).

Figure S5—Proportional extinction from simulations isolating the effect of continental configuration

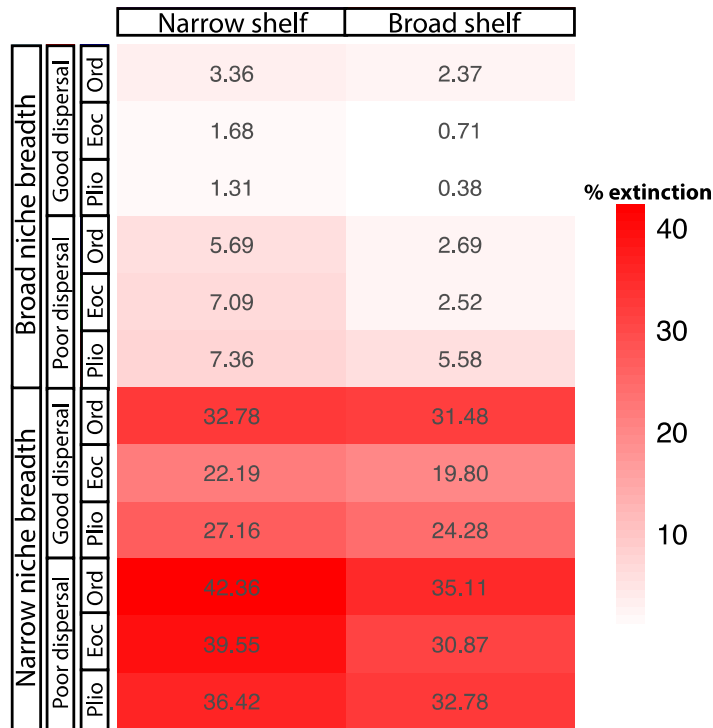| Broad niche breadth	Good dispersal		Narrow shelf	Broad shelf
		Ord	3.36	2.37
		Eoc	1.68	0.71
		Plio	1.31	0.38
	Poor dispersal	Ord	5.69	2.69
		Eoc	7.09	2.52
		Plio	7.36	5.58
Narrow niche breadth	Good dispersal	Ord	32.78	31.48
		Eoc	22.19	19.80
		Plio	27.16	24.28
	Poor dispersal	Ord	42.36	35.11
		Eoc	39.55	30.87
		Plio	36.42	32.78

% extinction: 40, 30, 20, 10

Figure S5. Proportional extinction (expressed as percentages for ease of reading) resulting from simulations when all else is held constant aside from continental configuration. Simulations were run in shallow marine shelf area directly adjacent to land, using a width of either one cell (narrow shelf) or three cells (broad shelf). All niche breadth and dispersal ability combinations are shown. Highest extinction intensities are obtained under the Late Ordovician paleogeographic reconstruction for all niche, dispersal, and continental shelf combinations, except under the broad continental shelf for species with broad niches and poor dispersal abilities. Eoc = Eocene; Ord = Ordovician; Plio = Pliocene.

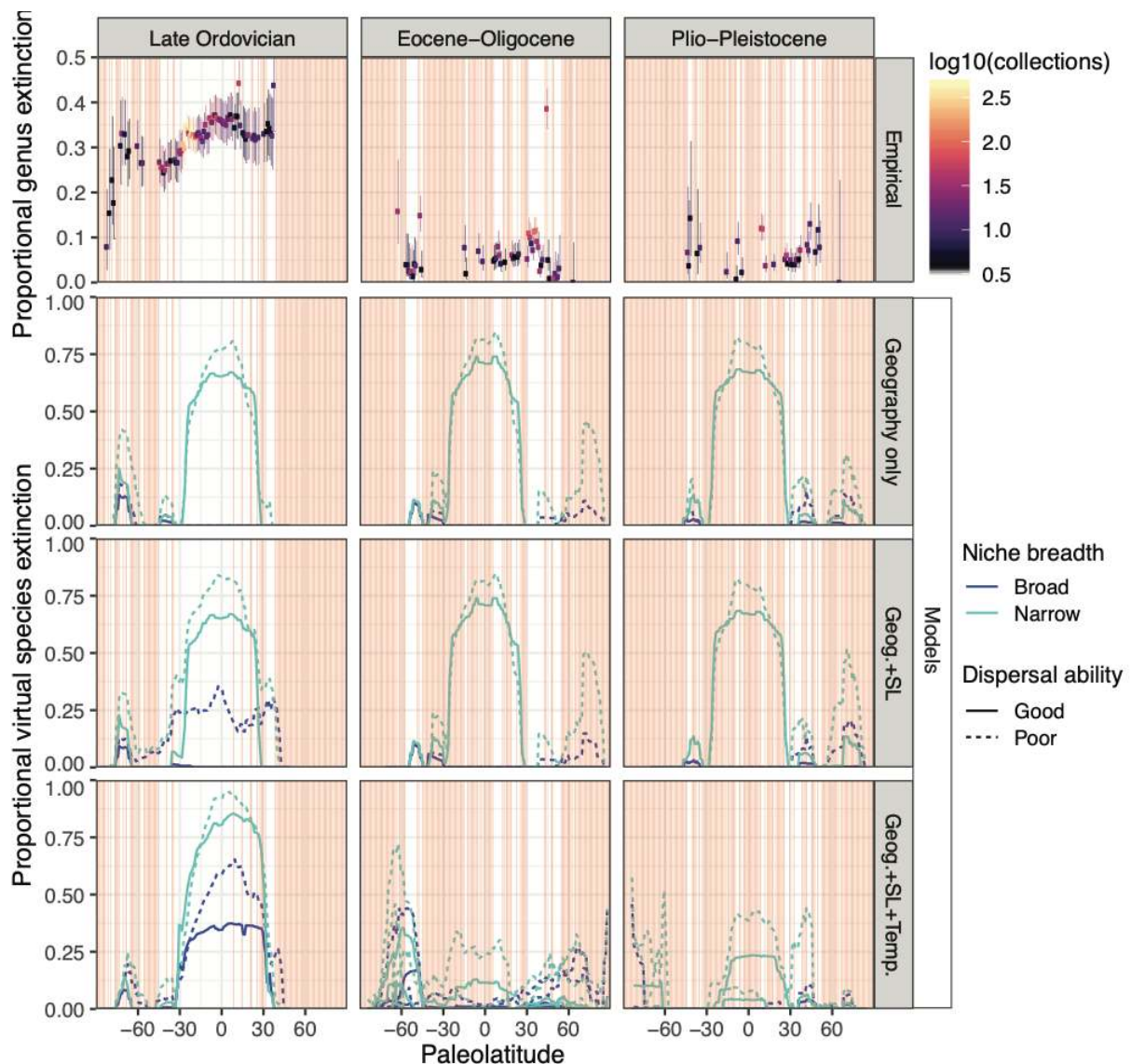# Figure S6—Proportional extinction by latitude

Figure S6. Top row: Observed proportional marine invertebrate genus extinction across paleolatitudes for the Late Ordovician, Eocene-Oligocene, and Plio-Pleistocene extinction events. Bottom three rows: Predicted proportional virtual species extinction for each event based on different modeling frameworks. Red shading indicates those latitudinal bands with no fossil data to compare to simulated data. "Geography only" simulations impose the same latitudinal temperature change across all three events. "Geog.+SL" simulations impose the same latitudinal temperature change across all three events but model changes in sea level. "Geog.+SL+Temp." simulations impose different temperature changes across all three events based on interval-specific AOGCMs. Observed extinctions based on analysis of marine invertebrate occurrences downloaded from the Paleobiology Database. Genera were assumed to be present at all paleolatitudes between the minimum and maximum paleolatitude at which they occur in a given interval. Error bars are 95% binomial confidence intervals. For predicted extinction patterns, color and type of lines indicate the niche breadths and dispersal abilities of simulated species. Results from runs based on different interval-specific AOGCMs and on different assumptions about the breadth of continental shelves/dispersal corridors were

19

averaged together. Note that upper panels show extinction of genera (potentially including multiple species with different ecological attributes), whereas lower panels model extinction of virtual species. Moreover, the Late Ordovician and Eocene FOAM AOGCMs do not incorporate changes in sea level. Thus, "Geog.+SL+Temp." simulations would likely produce even greater extinction if sea level and temperature effects were modelled jointly.

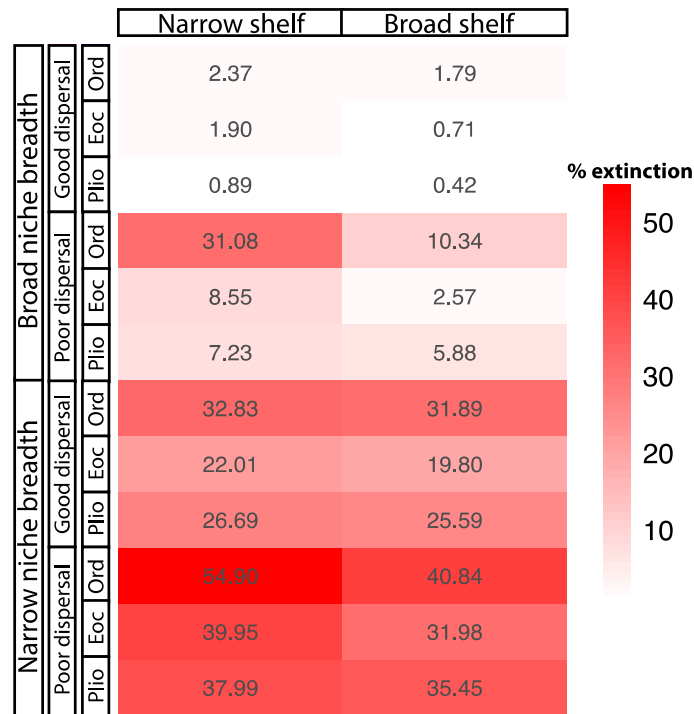| Niche breadth	Dispersal	Epoch	Narrow shelf	Broad shelf
Broad niche breadth	Good dispersal	Ord	2.37	1.79
		Eoc	1.90	0.71
		Plio	0.89	0.42
	Poor dispersal	Ord	31.08	10.34
		Eoc	8.55	2.57
		Plio	7.23	5.88
Narrow niche breadth	Good dispersal	Ord	32.83	31.89
		Eoc	22.01	19.80
		Plio	26.69	25.59
	Poor dispersal	Ord	54.90	40.84
		Eoc	39.95	31.98
		Plio	37.99	35.45

% extinction
50
40
30
20
10

Figure S7. Proportional extinction (expressed as percentages for ease of reading) from simulations that incorporate both paleogeography and estimated changes in sea level. Species were given one dispersal attempt to reach the new marine shelf position once sea level dropped. All niche breadth and dispersal ability combinations are shown. Highest extinction intensities are obtained under the Late Ordovician paleogeographic reconstruction for all niche, dispersal, and continental shelf combinations, except under the broad continental shelf for species with broad niches and poor dispersal abilities. Eoc = Eocene; Ord = Ordovician; Plio = Pliocene.

Figure S8—Proportional extinction from simulations isolating the effect of continental configuration & sea level change (five dispersal attempts)

				Narrow shelf	Broad s
Broad niche breadth	Good dispersal		Ord	0.00	0.0(
			Eoc	0.71	0.4!
			Plio	0.13	0.0(
	Poor dispersal		Ord	12.54	7.0?
			Eoc	4.92	1.8:
			Plio	4.19	3.3
Narrow niche breadth	Good dispersal		Ord	28.57	28.5
			Eoc	19.71	19.1
			Plio	22.93	22.8
	Poor dispersal		Ord	44.47	36.6
			Eoc	33.13	26.4
			Plio	33.04	30.3

Figure S8. Proportional extinction (expressed as percentages for ease of reading) from simulations that incorporate both paleogeography and estimated changes in sea level. Species were given five dispersal attempts to reach the new marine shelf position once sea level dropped. All niche breadth and dispersal ability combinations are shown. Highest extinction intensities are obtained under the Late Ordovician paleogeographic reconstruction for all niche, dispersal, and continental shelf combinations, except under the broad continental shelf for species with broad niches and poor dispersal abilities. Eoc = Eocene; Ord = Ordovician; Plio = Pliocene.

Figure S9—Proportional extinction from simulations using AOGCMs, climate model combinations [1-2] Late Ordovician, [3-6] Eocene–Oligocene, and [9-11] Pliocene–Pleistocene
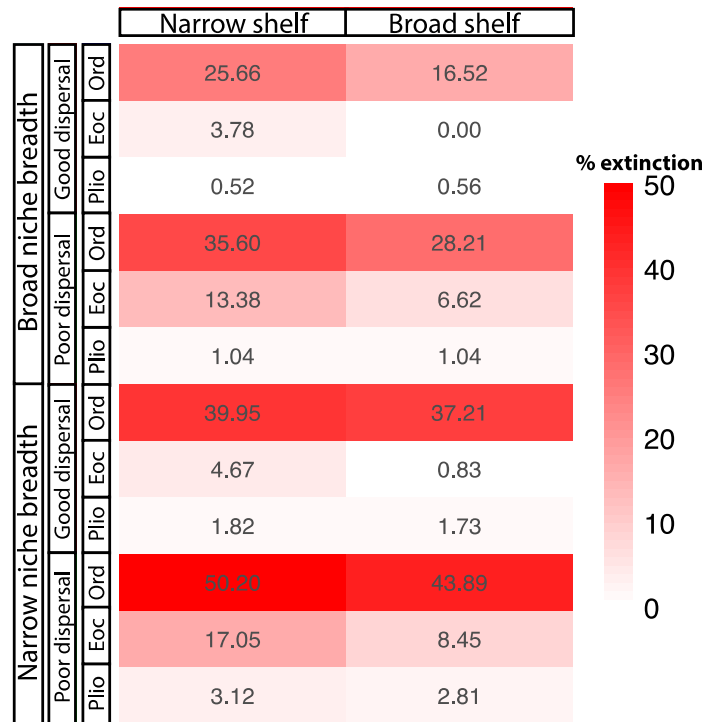

Figure S9. Proportional extinction (expressed as percentages for ease of reading) from simulations that incorporate interval-specific and paleogeographically-explicit surface temperature change estimates from AOGCMs. Results are shown for different AOGCM greenhouse-icehouse transitions, which are shown in square brackets and described in Table S3: Late Ordovician [1-2], Eocene–Oligocene [3-6], and Pliocene–Pleistocene [9-11]. All niche breadth, dispersal ability, and continental shelf combinations are shown. Highest extinction intensities are obtained for the Late Ordovician greenhouse-icehouse transition. Eoc = Eocene; Ord = Ordovician; Plio = Pliocene.

Figure S10—Proportional extinction from simulations using AOGCMs, climate model combinations [1-2] Late Ordovician, [4-7] Eocene–Oligocene, and [10-12] Pliocene–Pleistocene

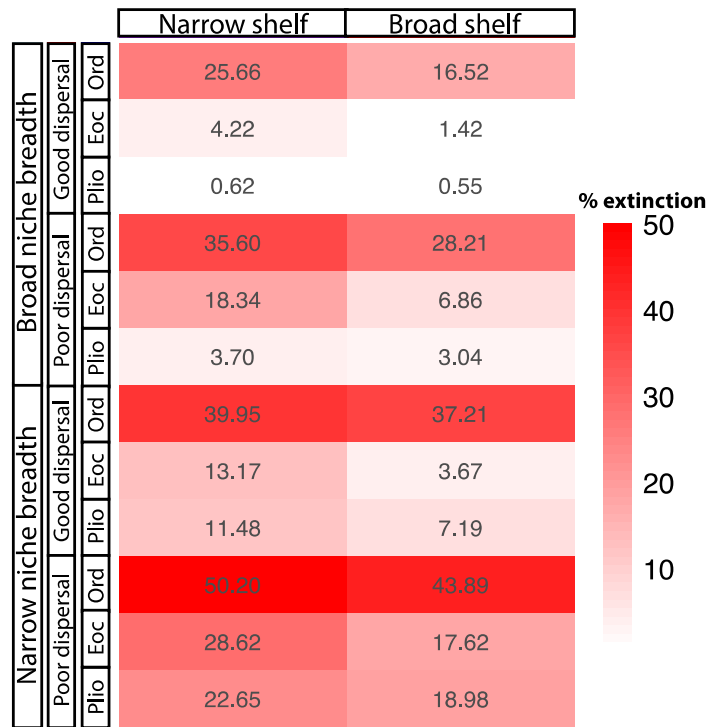|			Narrow shelf	Broad shelf
Broad niche breadth	Good dispersal	Ord	25.66	16.52
		Eoc	4.22	1.42
		Plio	0.62	0.55
	Poor dispersal	Ord	35.60	28.21
		Eoc	18.34	6.86
		Plio	3.70	3.04
Narrow niche breadth	Good dispersal	Ord	39.95	37.21
		Eoc	13.17	3.67
		Plio	11.48	7.19
	Poor dispersal	Ord	50.20	43.89
		Eoc	28.62	17.62
		Plio	22.65	18.98

% extinction: 50, 40, 30, 20, 10

Figure S10. Proportional extinction (expressed as percentages for ease of reading) from simulations that incorporate interval-specific and paleogeographically-explicit surface temperature change estimates from ocean-atmosphere general circulation models (AOGCMs), for combinations [1-2] Late Ordovician, [4-7] Eocene–Oligocene, and [10-12] Pliocene–Pleistocene. All niche breadth, dispersal ability, and continental shelf combinations are shown. Highest extinction intensities are obtained for the Late Ordovician greenhouse-icehouse transition. Eoc = Eocene; Ord = Ordovician; Plio = Pliocene.

Figure S11—Proportional extinction from simulations using AOGCMs, climate model combinations [1-2] Late Ordovician, [5-8] Eocene–Oligocene, and [10-12] Pliocene–Pleistocene

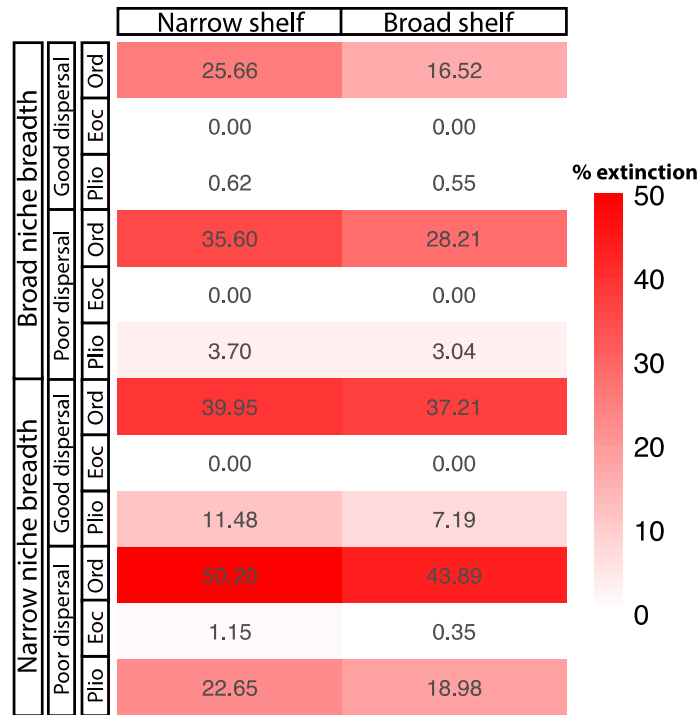|			Narrow shelf	Broad shelf
Broad niche breadth	Good dispersal	Ord	25.66	16.52
		Eoc	0.00	0.00
		Plio	0.62	0.55
	Poor dispersal	Ord	35.60	28.21
		Eoc	0.00	0.00
		Plio	3.70	3.04
Narrow niche breadth	Good dispersal	Ord	39.95	37.21
		Eoc	0.00	0.00
		Plio	11.48	7.19
	Poor dispersal	Ord	50.20	43.89
		Eoc	1.15	0.35
		Plio	22.65	18.98

% extinction
50
40
30
20
10
0

Figure S11. Proportional extinction (expressed as percentages for ease of reading) from simulations that incorporate interval-specific and paleogeographically-explicit surface temperature change estimates from ocean-atmosphere general circulation models (AOGCMs), for combinations [1-2] Late Ordovician, [5-8] Eocene–Oligocene, and [10-12] Pliocene–Pleistocene. All niche breadth, dispersal ability, and continental shelf combinations are shown. Highest extinction intensities are obtained for the Late Ordovician greenhouse-icehouse transition. Eoc = Eocene; Ord = Ordovician; Plio = Pliocene.

Figure S12—Proportional extinction from simulations using AOGCMs, climate model combinations [1-2] Late Ordovician, [5-8] Eocene–Oligocene, and [9-11] Pliocene–Pleistocene

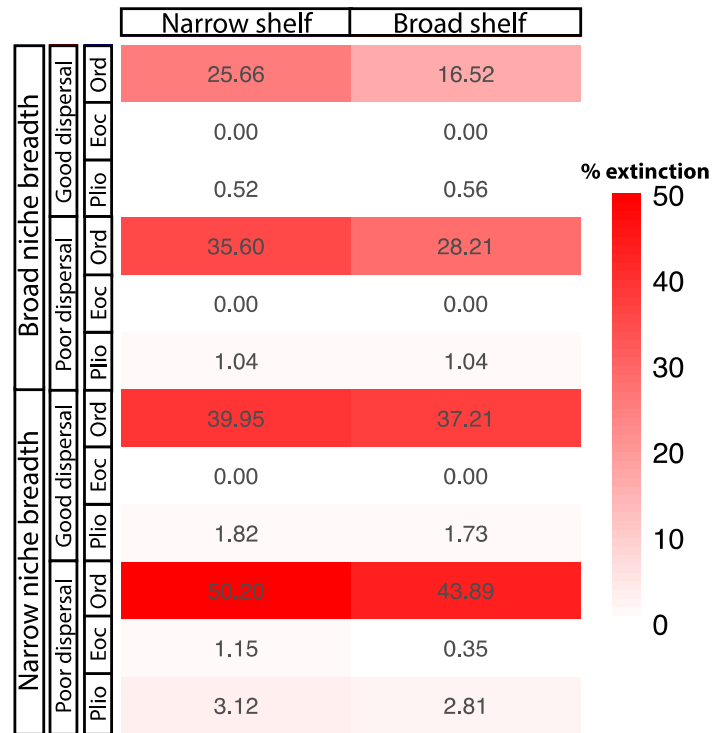|			Narrow shelf	Broad shelf
Broad niche breadth	Good dispersal	Ord	25.66	16.52
		Eoc	0.00	0.00
		Plio	0.52	0.56
	Poor dispersal	Ord	35.60	28.21
		Eoc	0.00	0.00
		Plio	1.04	1.04
Narrow niche breadth	Good dispersal	Ord	39.95	37.21
		Eoc	0.00	0.00
		Plio	1.82	1.73
	Poor dispersal	Ord	50.20	43.89
		Eoc	1.15	0.35
		Plio	3.12	2.81

% extinction: 50, 40, 30, 20, 10, 0

Figure S12. Proportional extinction (expressed as percentages for ease of reading) from simulations that incorporate interval-specific and paleogeographically-explicit surface temperature change estimates from ocean-atmosphere general circulation models (AOGCMs), for combinations [1-2] Late Ordovician, [5-8] Eocene–Oligocene, and [9-11] Pliocene–Pleistocene. All niche breadth, dispersal ability, and continental shelf combinations are shown. Highest extinction intensities are obtained for the Late Ordovician greenhouse-icehouse transition. Eoc = Eocene; Ord = Ordovician; Plio = Pliocene.

Figure S13—Average latitudinal temperature change for the greenhouse-icehouse transitions from AOGCM combinations
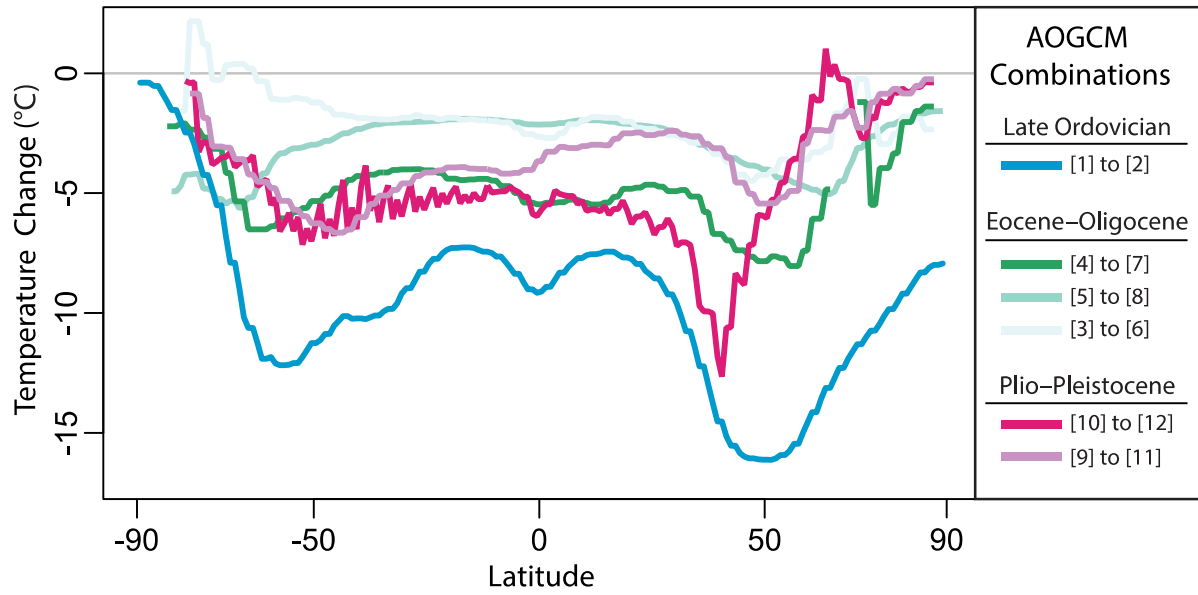

Figure S13. Average latitudinal temperature change from greenhouse to icehouse conditions, shown every 1° latitude, dervied from AOGCM model pairings. AOGCMs used to represent each climate transition for the Late Ordovician, Eocene–Oligocene, and Pliocene–Pleistocene are represented in square brackets (see Table S3).

Figure S14— Comparison of mean change in SST predicted by AOGCMs and by geochemical proxies
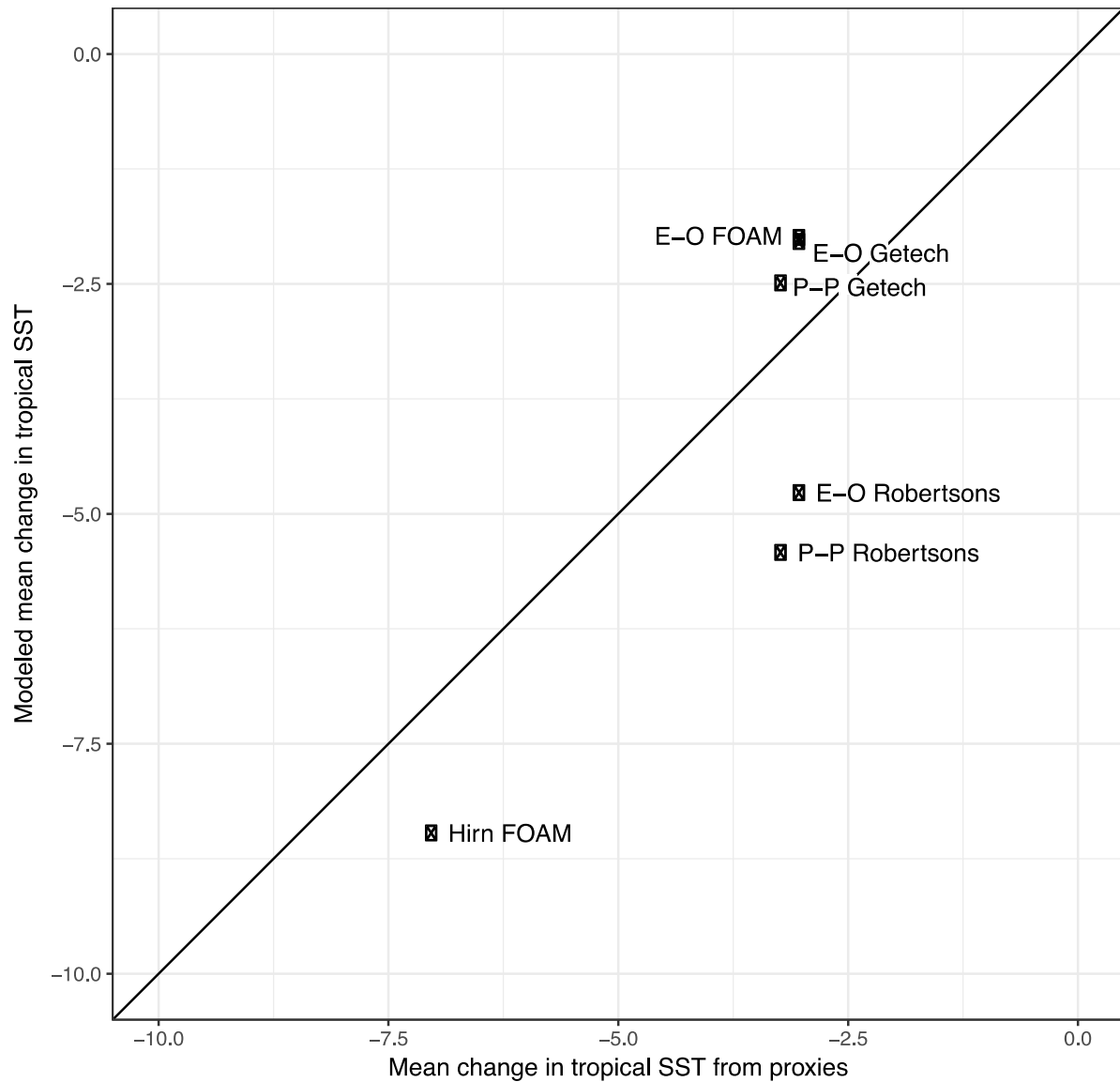

Figure S14. Comparison of the mean change in tropical sea surface temperature (SST) predicted by AOGCMs (see Table S3) and inferred from geochemical proxies for the Late Ordovician, Eocene–Oligocene, and Plio-Pleistocene cooling events. Proxy estimates come from Finnegan et al.[16] for the Late Ordovician, Liu et al.[29], Lear et al.[19], and Katz et al.[62] for the Eocene–Oligocene, and from Herbert et al.[30] for the Plio-Pleistocene.
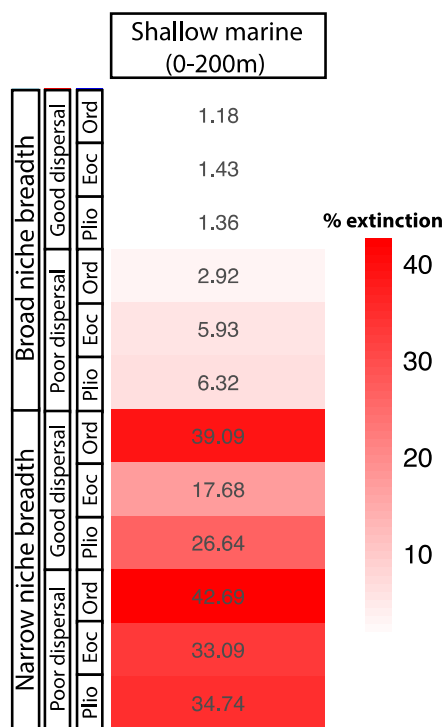
Figure S15. Proportional extinction (expressed as percentages for ease of reading) resulting from simulations when all else is held constant aside from continental configuration, run in shallow marine area defined as cells within 0 to 200 m water depth. Highest extinction intensities are obtained under the Late Ordovician paleogeographic reconstruction for species with narrow niche breadths. Eoc = Eocene; Ord = Ordovician; Plio = Pliocene.

Figure S16—Proportional extinction from simulations isolating the effect of continental configuration & sea level change, using a shelf definition of 0–200 m water depth
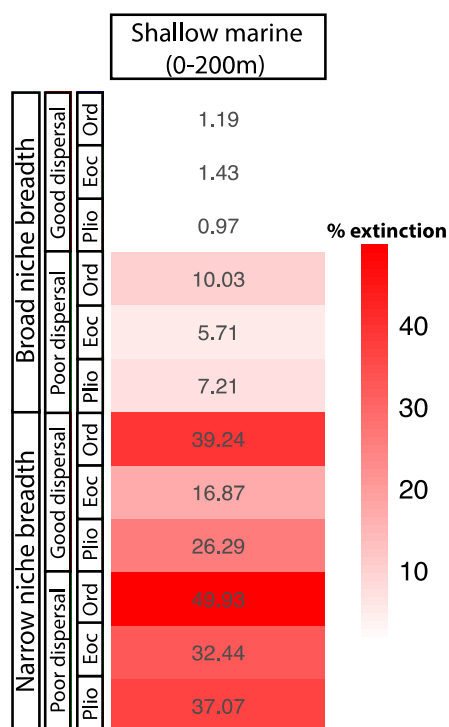

Figure S16. Proportional extinction (expressed as percentages for ease of reading) from simulations that incorporate both paleogeography and estimated changes in continental flooding, run in shallow marine area defined as cells within 0 to 200 m water depth. Species were given one dispersal attempt to reach the new marine shelf position once sea level dropped. Highest extinction intensities are obtained under the Late Ordovician paleogeographic reconstruction for all niche and dispersal combinations, except for species with broad niches and good dispersal abilities. Eoc = Eocene; Ord = Ordovician; Plio = Pliocene.

Figure S17—Proportional extinction from simulations using AOGCMs, using a shelf definition of 0–200 m water depth
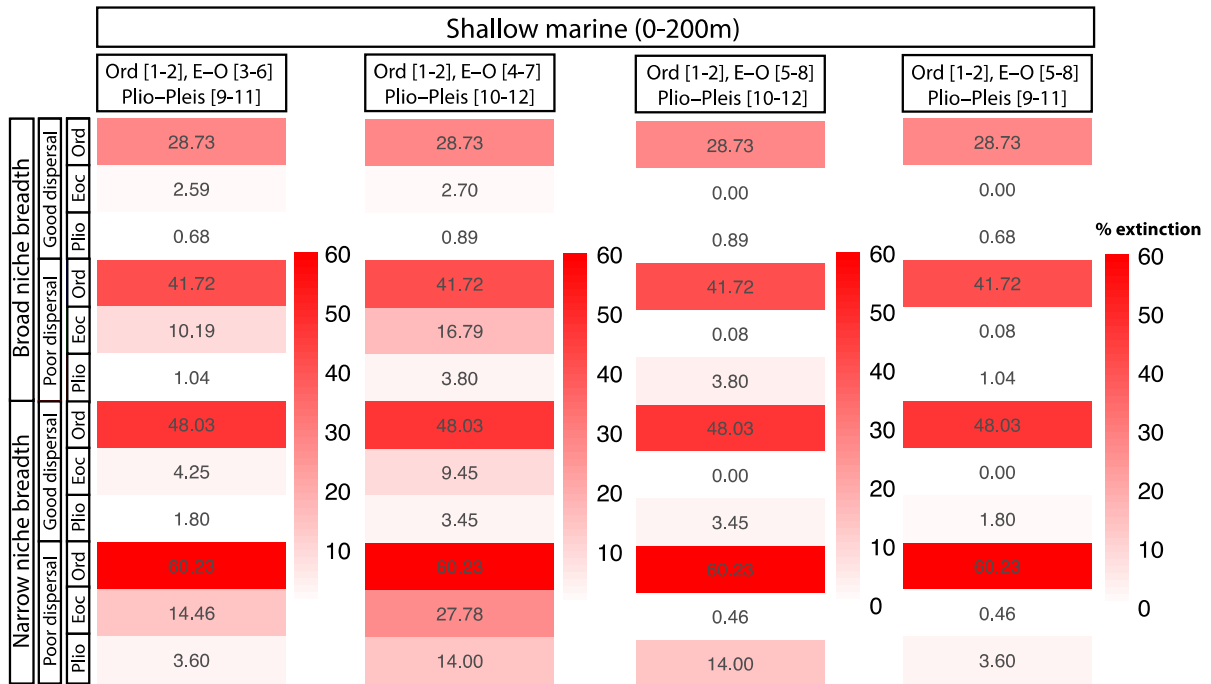

Figure S17. Proportional extinction (expressed as percentages for ease of reading) from simulations that incorporate interval-specific and paleogeographically-explicit surface temperature change estimates from ocean-atmosphere general circulation models (AOGCMs), run in shallow marine area defined as cells within 0 to 200 m water depth. AOGCMs model combinations are indicated in square brackets (see Table S3). Highest extinction intensities are obtained for the Late Ordovician greenhouse-icehouse transition. Eoc = Eocene; E–O = Eocene to Oligocene transition; Ord = Ordovician; Plio = Pliocene; Plio–Pleis = Pliocene to Pleisotcene transition.

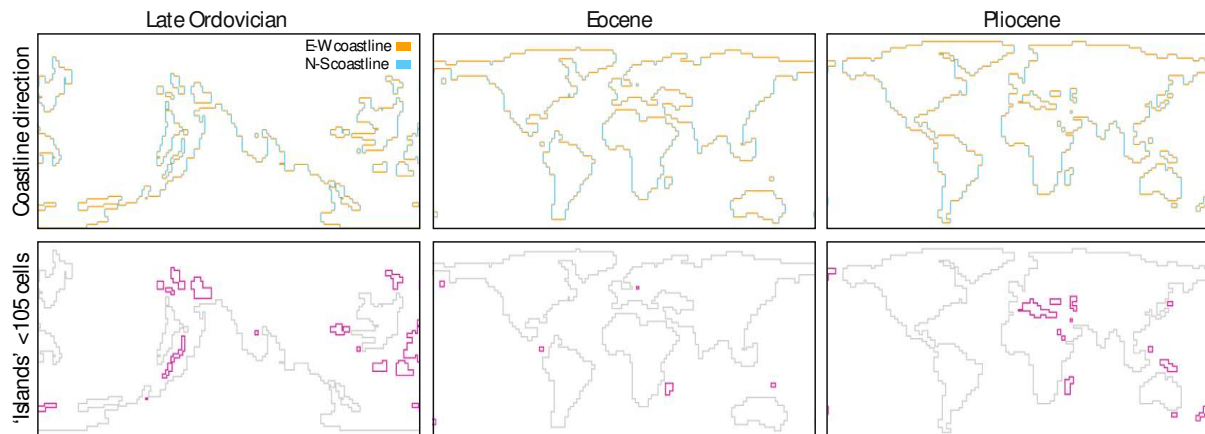# Figure S18—Definition of coastline orientation and small islands

Figure S18. Identification of coastline orientation (top panels) and small 'islands' (bottom panels) to characterise proportional extinction for three paleogeographies. East-west (E-W) coastlines are depicted in orange and north-south (N-S) coastlines in blue. 'Corner' cells are shown in gray. We examined the effect of small isolated shallow marine shelf areas only (i.e., small 'islands'), since the entirety of a small 'island' is more likely to become unsuitable for a species when climate changes and to prohibit habitat tracking. Only 'islands' containing fewer than 105 cells were selected, shown in pink. Details on specific methodology are provided in S.1.3.4.

References

1   Qiao, H., Saupe, E. E., Soberón, J., Peterson, A. T. & Myers, C. E. Impacts of niche breadth and dispersal ability on macroevolutionary patterns. *The American Naturalist* **188**, 149-162 (2016).

2   Rangel, T. F. L., Diniz-Filho, J. A. F. & Colwell, R. K. Species richness and evolutionary niche dynamics: a spatial pattern–oriented simulation experiment. *The American Naturalist* **170**, 602-616 (2007).

3   Saupe, E. E. *et al.* Non-random latitudinal gradients in range size and niche breadth predicted by spatial patterns of climate. *Glob Ecol Biogeogr* (2019).

4   Tomašových, A., Jablonski, D., Berke, S. K., Krug, A. Z. & Valentine, J. W. Nonlinear thermal gradients shape broad-scale patterns in geographic range size and can reverse Rapoport's rule. *Glob Ecol Biogeogr* **24**, 157-167 (2015).

5   Blakey, R. C. *Colorado Plateau Geosystems, 1–1*, <http://cpgeosystems.com > (2016).

6   Scotese, C. Digital Paleogeographic Map Archive on CD-ROM, PALEOMAP Project, Arlington, Texas. (2001).

7   Harris, J. *et al.* in *Petroleum Systems Analysis—Case Studies: AAPG Memoir* Vol. 114 (eds M A AbuAli, I Moretti, & H M Nordgård Bolås) 37-60 (2017).

8   Stuart-Smith, R. D., Edgar, G. J. & Bates, A. E. Thermal limits to the geographic distributions of shallow-water marine species. *Nature Ecology & Evolution* **1**, 1846–1852 (2017).

9   Sunday, J. M., Bates, A. E. & Dulvy, N. K. Global analysis of thermal tolerance and latitude in ectotherms. *Proceedings of the Royal Society of London B: Biological Sciences* **278**, 1823-1830 (2010).

10   McClain, C. R., Stegen, J. C. & Hurlbert, A. H. Dispersal, environmental niches and oceanic-scale turnover in deep-sea bivalves. *Proceedings of the Royal Society of London B* **rspb20112166** (2011).

11   Van Wyngaarden, M. *et al.* Identifying patterns of dispersal, connectivity and selection in the sea scallop, *Placopecten magellanicus*, using RADseq-derived SNPs. *Evolutionary Applications* **10**, 102-117 (2017).

12   Liow, L. H. & Stenseth, N. C. The rise and fall of species: implications for macroevolutionary and macroecological studies. *Proceedings of the Royal Society of London B* **274**, 2745-2752 (2007).

13   Webb, T. J. & Gaston, K. J. Geographic range size and evolutionary age in birds. *Proceedings of the Royal Society of London B* **267**, 1843-1850 (2000).

14   Hothorn, T., Bretz, F. & Westfall, P. Simultaneous inference in general parametric models. *Biom J* **50**, 346-363 (2008).

15   Hahsler, M. & Piekenbrock, M. dbscan: Density Based Clustering of Applications with Noise (DBSCAN) and Related Algorithms. R package version 1.1-1. *https://CRAN.R-project.org/package=dbscan* (2017).

16   Finnegan, S. *et al.* The magnitude and duration of Late Ordovician-Early Silurian glaciation. *Science* **331**, 903-906 (2011).

17   Loi, A. *et al.* The Late Ordovician glacio-eustatic record from a high-latitude storm-dominated shelf succession: the Bou Ingarf section (Anti-Atlas, Southern Morocco). *Palaeogeography, Palaeoclimatology, Palaeoecology* **296**, 332-358 (2010).

18	Pohl, A. *et al.* Glacial onset predated Late Ordovician climate cooling. *Paleoceanography* **31**, 800-821 (2016).

19	Lear, C. H., Bailey, T. R., Pearson, P. N., Coxall, H. K. & Rosenthal, Y. Cooling and ice growth across the Eocene-Oligocene transition. *Geo* **36**, 251-254 (2008).

20	Pusz, A. E., Thunell, R. C. & Miller, K. G. Deep water temperature, carbonate ion, and ice volume changes across the Eocene-Oligocene climate transition. *Paleoceanography and Paleoclimatology* **26**, PA2205 (2011).

21	Pekar, S. F. & Christie-Blick, N. Resolving apparent conflicts between oceanographic and Antarctic climate records and evidence for a decrease in pCO2 during the Oligocene through early Miocene (34–16 Ma). *Palaeogeography, Palaeoclimatology, Palaeoecology* **260**, 41-49 (2008).

22	Houben, A. J., van Mourik, C. A., Montanari, A., Coccioni, R. & Brinkhuis, H. The Eocene–Oligocene transition: Changes in sea level, temperature or both? *Palaeogeography, Palaeoclimatology, Palaeoecology* **335**, 75-83 (2012).

23	Ladant, J. B., Donnadieu, Y., Lefebvre, V. & Dumas, C. The respective role of atmospheric carbon dioxide and orbital parameters on ice sheet evolution at the Eocene-Oligocene transition. *Paleoceanography* **29**, 810-823 (2014).

24	Wilson, D. S., Pollard, D., DeConto, R. M., Jamieson, S. S. & Luyendyk, B. P. Initiation of the West Antarctic Ice Sheet and estimates of total Antarctic ice volume in the earliest Oligocene. *Geophys. Res. Lett.* **40**, 4305-4309 (2013).

25	Stocchi, P. *et al.* Relative sea-level rise around East Antarctica during Oligocene glaciation. *Nature Geoscience* **6**, 380, doi:10.1038/ngeo1783 https://www.nature.com/articles/ngeo1783#supplementary-information (2013).

26	Pohl, A. & Austermann, J. A sea-level fingerprint of the Late Ordovician ice-sheet collapse. *Geo* **46**, 595-598 (2018).

27	Creveling, J. R., Finnegan, S., Mitrovica, J. X. & Bergmann, K. D. Spatial variation in Late Ordovician glacioeustatic sea-level change. *Earth Planet Sci Lett* **496**, 1-9 (2018).

28	Bergmann, K. D. *et al.* A paired apatite and calcite clumped isotope thermometry approach to estimating Cambro-Ordovician seawater temperatures and isotopic composition. *Geochim Cosmochim Acta* **224**, 18-41 (2018).

29	Liu, Z. H. *et al.* Global cooling during the Eocene-Oligocene climate transition. *Science* **323**, 1187-1190 (2009).

30	Herbert, T. D., Peterson, L. C., Lawrence, K. T. & Liu, Z. Tropical ocean temperatures over the past 3.5 million years. *Science* **328**, 1530-1534 (2010).

31	Lunt, D. J. *et al.* Palaeogeographic controls on climate and proxy interpretation. *Climates of the Past* **12**, 1181-1198 (2016).

32	Valdes, P. J. *et al.* The BRIDGE HadCM3 family of climate models: HadCM3@Bristol v1.0. *Geoscience Model Development* **10**, 3715-3743 (2017).

33	Cox, P. M., Huntingford, C. & Harding, R. J. A canopy conductance and photosynthesis model for use in a GCM land surface scheme. *JHyd* **212-213**, 79-94 (1998).

34	Cox, P. M., Betts, R. A., Jones, C. D., Spall, S. A. & Totterdell, I. J. in *Meteorology at the Millennium* (ed R Pearce) 259-279 (Academic Press, 2001).

35	Inglis, G. N. *et al.* Descent toward the Icehouse: Eocene sea surface cooling inferred from GDGT distributions. *Paleoceanography* **30**, 1000-1020 (2015).

36   Kennedy, A. T., Farnsworth, A., Lunt, D. J., Lear, C. H. & Markwick, P. J. Atmospheric and oceanic impacts of Antarctic glaciation across the Eocene–Oligocene transition. *Philosophical Transactions of the Royal Society, A* **373**, 20140419 (2015).

37   Li, S. *et al.* Oligocene climate signals and forcings in Eurasia revealed by plant macrofossil and modelling results. *Gondwana Res* **61**, 115-127 (2018).

38   Gough, D. O. Solar interior structure and luminosity variations. *SoPh* **74**, 21-34 (1981).

39   Pagani, M. *et al.* The role of carbon dioxide during the onset of Antarctic glaciation. *Science* **334**, 1261-1264 (2011).

40   Heureux, A. M. C. & Rickaby, R. E. M. Refining our estimate of atmospheric CO2 across the Eocene–Oligocene climatic transition. *Earth Planet Sci Lett* **409**, 329-338 (2015).

41   Pearson, P. N., Foster, G. L. & Wade, B. S. Atmospheric carbon dioxide through the Eocene-Oligocene climate transition. *Nature* **461**, 1110-1113 (2009).

42   Foster, G. L., Royer, D. L. & Lunt, D. J. Future climate forcing potentially without precedent in the last 420 million years. *Nature Communications* **8**, 14845 (2017).

43   Jacob, R. L. *Low frequency variability in a simulated atmosphere ocean system*, University of Wisconsin-Madison, (1997).

44   Dufresne, J. L. *et al.* Climate change projections using the IPSL-CM5 Earth System Model: from CMIP3 to CMIP5. *ClDy* **40**, 2123-2165 (2013).

45   Ritz, C., Rommelaere, V. & Dumas, C. Modeling the evolution of Antarctic ice sheet over the last 420,000 years: implications for altitude changes in the Vostok region. *JGR* **106**, 31943-31964 (2001).

46   Donnadieu, Y., Pucéat, E., Moiroud, M., Guillocheau, F. & Deconinck, J.-F. A better-ventilated ocean triggered by Late Cretaceous changes in continental configuration. *Nature Communication* **7**, 10316, doi:doi:10.1038/ncomms10316 (2016).

47   Poulsen, C. J. & Jacob, R. L. Factors that inhibit snowball Earth simulation. *Paleoceanography* **19**, PA4021, doi:doi:10.1029/2004PA001056 (2004).

48   Kiehl, J. T. *et al.* The national center for atmospheric research community climate model: CCM3. *JCli* **11**, 1131-1149 (1998).

49   Semtner, A. J. A model for the thermodynamic growth of sea ice in numerical investigations of climate. *JPO* **6**, 379-389 (1976).

50   Rubinstein, C. V., Gerrienne, P., la Puente, d. G. S., Astini, R. A. & Steemans, P. Early Middle Ordovician evidence for land plants in Argentina (eastern Gondwana). *New Phytol* **188**, 365-369 (2010).

51   Steemans, P. *et al.* Origin and radiation of the earliest vascular land plants. *Science* **324**, 353-353 (2009).

52   Edwards, D., Cherns, L. & Raven, J. A. Could land-based early photosynthesizing ecosystems have bioengineered the planet in mid-Palaeozoic times? *Palaeontology* **58**, 803-837 (2015).

53   Porada, P. *et al.* High potential for weathering and climate effects of non-vascular vegetation in the Late Ordovician. *Nature Communications* **7**, 12113 (2016).

54   Nardin, E. *et al.* Modeling the early Paleozoic long-term climatic trend. *Geol Soc Am Bull*, 1181-1192, doi:doi:10.1130/B30364.1 (2011).

55   Pohl, A., Donnadieu, Y., Le Hir, G., Buoncristiani, J. F. & Vennin, E. Effect of the Ordovician paleogeography on the (in)stability of the climate. *CliPa* **10**, 2053-2066 (2014).

56   Pohl, A., Nardin, E., Vandenbroucke, T. & Donnadieu, Y. High dependence of Ordovician ocean surface circulation on atmospheric CO2 levels. *Palaeogeography, Palaeoclimatology, Palaeoecology* **458**, 39-51 (2016).

57   Barrier, E. & Vrielynck, B. Palaeotectonic Maps of the Middle East, Commission for the Geologic Map of the World, Paris. (2008).

58   Lefebvre, V., Donnadieu, Y., Sepulchre, P., Swingedouw, D. & Zhang, Z. S. Deciphering the role of southern gateways and carbon dioxide on the onset of the Antarctic Circumpolar Current. *Paleoceanography* **24**, PA4201 (2012).

59   Wilson, D. S. *et al.* Antarctic topography at the Eocene-Oligocene boundary. *Palaeogeography, Palaeoclimatology, Palaeoecology* **335-336**, 24-34 (2012).

60   Bice, K., Barron, E. & Peterson, W. in *Tectonic Boundary Conditions for Climate Reconstructions*   212-226 (Oxford University Press, 1998).

61   Zachos, J. C., Pagani, M., Sloan, L., Thomas, E. & Billups, K. Trends, rhythms, and aberrations in global climate 65 Ma to present. *Science* **292**, 686-693 (2001).

62   Katz, M. E. *et al.* Stepwise transition from the Eocene greenhouse to the Oligocene icehouse. *Nature Geoscience* **1**, 329-334 (2008).